GEOPHYSICS, VOL. 78, NO. 1 (JANUARY-FEBRUARY 2013); P. T29–T39, 7 FIGS., 1 TABLE.
10.1190/GEO2012-0062.1

Application of perfectly matched layer for scalar arbitrarily wide-angle wave equations

Hanming Chen[1], Hui Zhou[1], He Lin[1], and Shangxu Wang[1]

ABSTRACT

Arbitrarily wide-angle wave equation (AWWE) is a space domain, high-order one-way wave equation (OWWE). Its accuracy can be arbitrarily increased, and it is amenable to easy numerical implementation. Those properties make it outstanding among the existing OWWEs and further enable it to be a desirable tool for migration. We extend the perfectly matched layer (PML) to 3D scalar AWWE to provide a good approach to suppress artifacts arising at truncation boundaries. We follow the concept of complex coordinate stretching, and the derivation procedure of PML for AWWE is straightforward. An existing finite-difference scheme is adopted to fit the split PML formulation and its stability is observed through numerical examples. The performance of the developed PML condition is compared with two different wave-equation based absorbing boundary conditions. Numerical results illustrate that the PML condition used in AWWE propagator can effectively absorb the propagating waves and evanescent waves at a price of limited additional computation cost.

INTRODUCTION

Wave equation-based migration methods are more effective in imaging complex structures compared with ray-based (Kirchhoff) method. Those wave equation-based methods can be further classified into one-way wave equation (OWWE) migration and reverse-time migration (RTM) (Baysal et al., 1983; McMechan, 1983; Whitmore, 1983). RTM has a stronger ability to image complex geologic structures (e.g., salt flanks) than OWWE but produces more artifacts in the images. Meanwhile, RTM has a high computation cost, especially in 3D cases, which delays its wide application in practice (Mulder and Plessix, 2004). Therefore, those cheaper migration methods employing OWWEs are still in use (e.g., Zhang et al., 2006; Bakker, 2009; Jia and Wu, 2009).

The early OWWEs represented in the wavenumber domain, such as phase shift (Gazdag, 1978), are only applicable to vertically layered media. To consider laterally varying velocity, some correction schemes were proposed, e.g., phase shift plus interpolation (PSPI) (Gazdag and Sguazzero, 1984), split-step Fourier method (SSF) (Stoffa et al., 1990), Fourier finite difference (FFD) (Ristow and Rühl, 1994), and its implicit scheme proposed by Biondi (2002). Other endeavors to generalize the principle of phase shift method to laterally inhomogeneous media can also be found, e.g., wide-angle screen propagators (Huang and Wu, 1996) and the hybrid pseudoscreen propagators (Jin et al., 1999).

Different from the OWWEs represented in the wavenumber domain, the versions in the space domain can handle arbitrarily varying velocity and that makes them to be more favored. However, space domain OWWE usually has two shortcomings, a limited accuracy and expensive computation cost. The famous 15° and 45° wave equations (Claerbout, 1985) have a relatively simple form, but their accuracy is insufficient to image steep dips. Subsequently, different high-order rational approximation schemes were used to develop OWWEs with a higher accuracy (e.g., Bamberger et al., 1988; Collins and Westwood, 1991). Some other researchers (e.g., Berkhout, 1979; Lee and Suh, 1985; Zhang, 1985) proposed various methods to improve the accuracy of OWWEs without significantly increasing the computation cost. A series of high-order OWWEs were also developed for modeling unbounded domains and they were summarized by Givoli (2004).

Among the newly developed high-order OWWEs, arbitrarily wide-angle wave equations (AWWEs) (Guddati, 2006) are outstanding in terms of accuracy and form. AWWEs are highly accurate space domain OWWEs and hence are applicable to heterogeneous media. According to the conclusions of Guddati and Heidari (2005), AWWEs can achieve an accurate coverage of up to 85° of dip angle, which is an attractive accuracy for migration. The form of AWWEs is very simple, only involving second-order partial derivatives, so

Manuscript received by the Editor 20 February 2012; revised manuscript received 31 August 2012; published online 11 December 2012.
[1]China University of Petroleum, State Key Laboratory of Petroleum Resource and Prospecting, CNPC Key Lab of Geophysical Exploration, Beijing, China. E-mail: huizhou@cup.edu.cn; huichanming@126.com; dujuan20061988@sina.com; wangsx@cup.edu.cn.

it is convenient to implement numerical calculations. Due to that, AWWEs have already been tested in migration (e.g., Guddati and Heidari, 2005; He et al., 2008; Sun and Du, 2011).

The kernel of wave equation-based migration is to numerically solve the wave equation, i.e., seismic forward modeling, in which absorbing boundary conditions (ABCs) are necessary to avoid edge reflections arising at the model's truncation boundaries. Numerous ABCs have been developed for that purpose, mainly including two categories: wave equation-based ABCs and material-based ABCs (Shlager and Schneider, 1995). The former are actually based on OWWEs which make use of the directions of propagating waves. Similar to development of OWWEs for migration, the wave equation-based ABCs also evolve from low-order schemes (e.g., Clayton and Engquist, 1977; Engquist and Majda, 1977; Mur, 1981) into high-order ones (e.g., Grote and Keller, 1996; Rowley and Colonius, 2000; Givoli and Neta, 2003). Note that AWWEs are essentially equivalent to a high-order ABC, the continued-fraction absorbing boundary condition (CFABC), proposed by Guddati and Tassoulas (2000).

Regarding the material-based ABCs, the perfectly matched layer (PML) (Bérenger, 1994) is undoubtedly the most robust one. An easy way to understand PML was provided by Chew and Weedon (1994) who showed that PML can be realized by a complex coordinate stretching. In view of such an interpretation, PML were successfully extended to second-order seismic wave equation (e.g., Komatitsch and Tromp, 2003; Yuan et al., 2011).

It is worth mentioning that PML and high-order ABCs seem to be two different approaches, but in fact they have an intimate connection. Asvadurov et al. (2003) found that the minimal impedance error of discretized PML can be achieved by using a purely imaginary coordinate stretching rather than a complex one. In that condition, the PML discretization is algebraically equivalent to the rational approximation of the square root, which is the basic idea of developing high-order ABCs. Guddati and Lim (2006) further illustrate the relationship between the high-order scheme and PML with a special finite-element discretization. They conclude that a purely imaginary element length is optimal for absorbing the propagating wave mode, whereas a complex imaginary element length that is consistent with the PML scheme, is simultaneously effective for the propagating wave mode and evanescent wave mode.

Although so many ABCs have been proposed for full wave equation, only relatively few of them can be directly used for OWWEs. Some variations based on their counterparts for full wave equation were developed (e.g., Clayton and Engquist, 1980; Zhou and McMechan, 2000). A handful of applications of PML for OWWEs in the frequency domain can also be found (e.g., Collino, 1997; Levy, 2001; Lu and Zhu, 2007).

In this article, we extend the PML boundary condition to 3D time-space domain scalar AWWE to suppress undesired edge reflections in AWWE forward modeling. The performance of the derived PML scheme is compared with the second-order paraxial wave equation (abbreviated CE2) (Clayton and Engquist, 1977) and the highly accurate absorbing boundary condition (HABC) proposed by Heidari and Guddati (2006) for 2D scalar AWWEs. The finite-difference scheme presented by Guddati and Heidari (2005) is adopted to fit the split PML formulation. The stability of the explicit difference scheme in the interior region and the PML regions is monitored through numerical examples. Finally, some conclusions are realized.

METHOD

Formulations

The 3D scalar downward-propagating AWWEs take the form (Guddati and Heidari, 2005)

$$-\mathbf{d}\frac{\partial^2 u}{\partial z \partial t}-\frac{1}{c}(\mathbf{\Lambda}_1+\mathbf{\Lambda}_2)\frac{\partial^2 \mathbf{u}}{\partial t^2}+c\mathbf{\Lambda}_2\frac{\partial^2 \mathbf{u}}{\partial x^2}c\mathbf{\Lambda}_2\frac{\partial^2 \mathbf{u}}{\partial y^2}=\mathbf{0}, \quad (1)$$

where

$$\mathbf{\Lambda}_1=\frac{c}{2}\begin{bmatrix} \frac{1}{c_1} & -\frac{1}{c_1} & & & & \\ -\frac{1}{c_1} & \frac{1}{c_1}+\frac{1}{c_2} & -\frac{1}{c_2} & & & \\ & -\frac{1}{c_2} & \ddots & \ddots & & \\ & & \ddots & \ddots & & \\ & & & & \frac{1}{c_{n-2}}+\frac{1}{c_{n-1}} & -\frac{1}{c_{n-1}} \\ & & & & -\frac{1}{c_{n-1}} & \frac{1}{c_{n-1}}+\frac{1}{c_n} \end{bmatrix}_{n\times n}, \quad (2)$$

$$\mathbf{\Lambda}_2=\frac{1}{2c}\begin{bmatrix} c_1 & c_1 & & & & \\ c_1 & c_1+c_2 & c_2 & & & \\ & c_2 & \ddots & \ddots & & \\ & & \ddots & \ddots & & \\ & & & & c_{n-2}+c_{n-1} & c_{n-1} \\ & & & & c_{n-1} & c_{n-1}+c_n \end{bmatrix}_{n\times n}, \quad (3)$$

with $\mathbf{d}=(1,0,\cdots,0)_{1\times n}$ and $\mathbf{u}=(u,u_1,\cdots,u_{n-1})^T$. The superscript T denotes transposition and n represents the number of equations. Note that the first component of $\mathbf{u}$, i.e., the scalar u is what we need and the remaining components are auxiliary variables. c and c_i $(i=1,2,...,n)$ are, respectively, background velocity and reference velocities.

The accuracy of AWWEs is affected by the number of auxiliary variables and setting of the reference velocities. Each reference velocity c_i determines a specific propagating angle θ_i ($\cos\theta_i=\frac{c}{c_i}$) measured from the vertical axis, with which the dispersion curve of AWWEs accurately matches that of the exact OWWE. One auxiliary variable with two reference velocities $(c,4c)$ and two auxiliary variables with three appropriate reference velocities can be expected to achieve a very good imaging. When no auxiliary variable is used, AWWE degrades to the 15° wave equation. Regarding the computational cost, the AWWE propagator with one auxiliary variable only consumes a computing time about two times the 15° wave equation, but significantly improves the imaging quality (Guddati and Heidari, 2005).

Starting from equation 1, we attempt to construct a corresponding PML formulation. Assuming the positive z-axis is downward and considering attenuations along the x- and y-axis simultaneously, the vector $\mathbf{u}$ is split into three terms to obtain

$$\begin{cases} \frac{1}{c}(\mathbf{\Lambda}_1+\mathbf{\Lambda}_2)\frac{\partial^2\mathbf{u}_1}{\partial t^2}=c\mathbf{\Lambda}_2\frac{\partial^2\mathbf{u}}{\partial x^2} \\ \frac{1}{c}(\mathbf{\Lambda}_1+\mathbf{\Lambda}_2)\frac{\partial^2\mathbf{u}_2}{\partial t^2}=c\mathbf{\Lambda}_2\frac{\partial^2\mathbf{u}}{\partial y^2} \\ \frac{1}{c}(\mathbf{\Lambda}_1+\mathbf{\Lambda}_2)\frac{\partial^2\mathbf{u}_3}{\partial t^2}=-\mathbf{d}\frac{\partial^2 u}{\partial z\partial t} \end{cases}. \tag{4}$$

Then the first two formulas of equation 4 are transformed into the frequency domain

$$\begin{cases} \frac{(i\omega)^2}{c}(\mathbf{\Lambda}_1+\mathbf{\Lambda}_2)\tilde{\mathbf{u}}_1=c\mathbf{\Lambda}_2\frac{\partial^2\tilde{\mathbf{u}}}{\partial x^2} \\ \frac{(i\omega)^2}{c}(\mathbf{\Lambda}_1+\mathbf{\Lambda}_2)\tilde{\mathbf{u}}_2=c\mathbf{\Lambda}_2\frac{\partial^2\tilde{\mathbf{u}}}{\partial y^2} \end{cases}, \tag{5}$$

where $\tilde{\mathbf{u}}$, $\tilde{\mathbf{u}}_1$, and $\tilde{\mathbf{u}}_2$ are the corresponding Fourier transform of $\mathbf{u}$, $\mathbf{u}_1$, and $\mathbf{u}_2$, and ω is angle frequency. Note that the third formula of equation 4 is kept unchanged because equation 1 represents a downward-propagating wave equation and no attenuation is required along the z-axis. The next step is to replace x and y in equation 5 with following complex variables

$$\begin{cases} \tilde{x}=x-\frac{i}{\omega}\int_0^x d_x(s)ds \\ \tilde{y}=y-\frac{i}{\omega}\int_0^y d_y(s)ds \end{cases}, \tag{6}$$

where $d_x(x)$ and $d_y(y)$ represent the damping functions in the PML regions. After using the chain rule

$$\begin{cases} \frac{\partial f}{\partial\tilde{x}}=\frac{\partial f}{\partial x}\frac{\partial x}{\partial\tilde{x}}=\frac{i\omega}{i\omega+d_x(x)}\frac{\partial f}{\partial x} \\ \frac{\partial f}{\partial\tilde{y}}=\frac{\partial f}{\partial y}\frac{\partial y}{\partial\tilde{y}}=\frac{i\omega}{i\omega+d_y(y)}\frac{\partial f}{\partial y} \end{cases}, \tag{7}$$

equation 5 with damping functions in the frequency domain can be written as

$$\begin{cases} \frac{(i\omega)^2}{c}(\mathbf{\Lambda}_1+\mathbf{\Lambda}_2)\tilde{\mathbf{u}}_1=c\mathbf{\Lambda}_2\left\{\frac{(i\omega)^2}{[i\omega+d_x(x)]^2}\frac{\partial^2\tilde{\mathbf{u}}}{\partial x^2}-\frac{\partial d_x(x)}{\partial x}\frac{(i\omega)^2}{[i\omega+d_x(x)]^3}\frac{\partial\tilde{\mathbf{u}}}{\partial x}\right\} \\ \frac{(i\omega)^2}{c}(\mathbf{\Lambda}_1+\mathbf{\Lambda}_2)\tilde{\mathbf{u}}_2=c\mathbf{\Lambda}_2\left\{\frac{(i\omega)^2}{[i\omega+d_y(y)]^2}\frac{\partial^2\tilde{\mathbf{u}}}{\partial y^2}-\frac{\partial d_y(y)}{\partial y}\frac{(i\omega)^2}{[i\omega+d_y(y)]^3}\frac{\partial\tilde{\mathbf{u}}}{\partial y}\right\} \end{cases}. \tag{8}$$

The corresponding time domain version can be obtained by the inverse Fourier transform,

$$\begin{cases} \left[\frac{\partial}{\partial t}+d_x(x)\right]^2(\mathbf{\Lambda}_1+\mathbf{\Lambda}_2)\mathbf{u}_1=c^2\mathbf{\Lambda}_2\left\{\frac{\partial^2\mathbf{u}}{\partial x^2}-\frac{\partial d_x(x)}{\partial x}\exp[-d_x(x)t]*\frac{\partial\mathbf{u}}{\partial x}\right\} \\ \left[\frac{\partial}{\partial t}+d_y(y)\right]^2(\mathbf{\Lambda}_1+\mathbf{\Lambda}_2)\mathbf{u}_2=c^2\mathbf{\Lambda}_2\left\{\frac{\partial^2\mathbf{u}}{\partial y^2}-\frac{\partial d_y(y)}{\partial y}\exp[-d_y(y)t]*\frac{\partial\mathbf{u}}{\partial y}\right\} \end{cases}. \tag{9}$$

Write equation 9 together with the unchanged formula, i.e., the third formula of equation 4 to get a split PML formulation

$$\begin{cases} \left[\frac{\partial}{\partial t}+d_x(x)\right]^2(\mathbf{\Lambda}_1+\mathbf{\Lambda}_2)\mathbf{u}_1=c^2\mathbf{\Lambda}_2\left\{\frac{\partial^2\mathbf{u}}{\partial x^2}-\frac{\partial d_x(x)}{\partial x}\exp[-d_x(x)t]*\frac{\partial\mathbf{u}}{\partial x}\right\} \\ \left[\frac{\partial}{\partial t}+d_y(y)\right]^2(\mathbf{\Lambda}_1+\mathbf{\Lambda}_2)\mathbf{u}_2=c^2\mathbf{\Lambda}_2\left\{\frac{\partial^2\mathbf{u}}{\partial y^2}-\frac{\partial d_y(y)}{\partial y}\exp[-d_y(y)t]*\frac{\partial\mathbf{u}}{\partial y}\right\} \\ \frac{1}{c}(\mathbf{\Lambda}_1+\mathbf{\Lambda}_2)\frac{\partial^2\mathbf{u}_3}{\partial t^2}=-\mathbf{d}\frac{\partial^2 u}{\partial z\partial t} \end{cases}. \tag{10}$$

An exponential attenuation of the wavefield can be expected using equation 10 in the PML regions. By separately setting $d_x(x)=0$ or $d_y(y)=0$, attenuation along a single axis can be realized as well. It is true that the required memory and computation cost will increase due to the split formulation. Therefore, it is advisable to divide the whole computational domain into the interior region and PML regions, and then, respectively use the nonsplit formulation 1 and the split formulation 10 to update the wavefield.

Discretization

After obtaining equation 10, the next step is to solve it numerically in a stable and efficient way. Here, the finite-difference scheme proposed by Guddati and Heidari (2005) for equation 1 is adopted to fit the split PML formulation.

The solution domain is discretized such that

$$\mathbf{u}(x_i,y_j,z_k,t_n)=\mathbf{u}(i\Delta x,j\Delta y,k\Delta z,n\Delta t), \tag{11}$$

where Δx, Δy, Δz, and Δt are, respectively, the spatial and temporal increments. We use $\mathbf{u}^n(i,j,k)$ to represent $\mathbf{u}(i\Delta x,j\Delta y,k\Delta z,n\Delta t)$ and other variables are represented in the same way. The partial derivatives to x, y, and t in equation 1 are approximated using standard second-order centered difference operator. The Crank-Nicholson method is used to march in depth. Note that the center of difference approximation is located at $(i,j,k+\frac{1}{2})$. According to above approximation scheme, the discrete formula for updating $\mathbf{u}$ can be written as

$$\begin{aligned} &(\mathbf{\Lambda}_1+\mathbf{\Lambda}_2+\alpha_z\mathbf{D})\mathbf{u}^{n+1}\left(i,j,k+\frac{1}{2}\right) \\ &=\alpha_z\mathbf{d}\left[u^{n+1}(i,j,k)-u^{n-1}(i,j,k)+u^{n-1}\left(i,j,k+\frac{1}{2}\right)\right] \\ &\quad+(\mathbf{\Lambda}_1+\mathbf{\Lambda}_2)\left[2\mathbf{u}^n\left(i,j,k+\frac{1}{2}\right)-\mathbf{u}^{n-1}\left(i,j,k+\frac{1}{2}\right)\right] \\ &\quad+\alpha_x\mathbf{\Lambda}_2\left[\mathbf{u}^n\left(i+1,j,k+\frac{1}{2}\right)-2\mathbf{u}^n\left(i,j,k+\frac{1}{2}\right)\right. \\ &\quad\left.+\mathbf{u}^n\left(i-1,j,k+\frac{1}{2}\right)\right]+\alpha_y\mathbf{\Lambda}_2\left[\mathbf{u}^n\left(i,j+1,k+\frac{1}{2}\right)\right. \\ &\quad\left.-2\mathbf{u}^n\left(i,j,k+\frac{1}{2}\right)+\mathbf{u}^n\left(i,j-1,k+\frac{1}{2}\right)\right], \end{aligned} \tag{12}$$

and can be further expressed as

$$\begin{aligned} \mathbf{u}^{n+1}\left(i,j,k+\frac{1}{2}\right)&=\mathbf{h}_1\left[u^{n+1}(i,j,k)-u^{n-1}(i,j,k)+u^{n-1}\left(i,j,k+\frac{1}{2}\right)\right] \\ &+\mathbf{H}_2\left[2\mathbf{u}^n\left(i,j,k+\frac{1}{2}\right)-\mathbf{u}^{n-1}\left(i,j,k+\frac{1}{2}\right)\right] \\ &+\mathbf{H}_3\left\{\begin{array}{l}\alpha_x\left[\mathbf{u}^n\left(i+1,j,k+\frac{1}{2}\right)-2\mathbf{u}^n\left(i,j,k+\frac{1}{2}\right)+\mathbf{u}^n\left(i-1,j,k+\frac{1}{2}\right)\right] \\ +\alpha_y\left[\mathbf{u}^n\left(i,j+1,k+\frac{1}{2}\right)-2\mathbf{u}^n\left(i,j,k+\frac{1}{2}\right)+\mathbf{u}^n\left(i,j-1,k+\frac{1}{2}\right)\right]\end{array}\right\}, \end{aligned} \tag{13}$$

where

$$\begin{cases} \mathbf{h}_1=\alpha_z\mathbf{L}\mathbf{d},\mathbf{H}_2=\mathbf{L}(\mathbf{\Lambda}_1+\mathbf{\Lambda}_2) \\ \mathbf{H}_3=\mathbf{L}\mathbf{\Lambda}_2,\mathbf{L}=(\mathbf{\Lambda}_1+\mathbf{\Lambda}_2+\alpha_z\mathbf{D})^{-1},\mathbf{D}=\mathbf{d}^T\mathbf{d} \end{cases}, \tag{14}$$

and

$$\alpha_z = \frac{c\Delta t}{\Delta z}, \quad \alpha_x = \left(\frac{c\Delta t}{\Delta x}\right)^2, \quad \alpha_y = \left(\frac{c\Delta t}{\Delta y}\right)^2. \tag{15}$$

The value at $(i, j, k+1)$ is then obtained using the following relationship

$$\mathbf{u}(i,j,k+1) = 2\mathbf{u}\left(i,j,k+\frac{1}{2}\right) - \mathbf{u}(i,j,k). \tag{16}$$

Equations 13 and 16 are the explicit difference scheme for updating the wavefield in the interior region.

The same difference scheme is applied to approximate the partial derivatives in equation 10. The discrete formulas for updating $\mathbf{u}_1$ and $\mathbf{u}_2$ can be finally expressed as

$$\mathbf{u}_1^{n+1}\left(i,j,k+\frac{1}{2}\right) = \frac{1}{1+\Delta t d_x(i)} \left\{ \begin{array}{l} [2-\Delta t^2 d_x(i)^2]\mathbf{u}_1^n\left(i,j,k+\frac{1}{2}\right) \\ +[\Delta t d_x(i)-1]\mathbf{u}_1^{n-1}\left(i,j,k+\frac{1}{2}\right) \\ +\mathbf{H}_4\alpha_x \left[\begin{array}{l} \mathbf{u}^n\left(i+1,j,k+\frac{1}{2}\right) \\ 2\mathbf{u}^n\left(i,j,k+\frac{1}{2}\right) \\ +\mathbf{u}^n\left(i-1,j,k+\frac{1}{2}\right) \end{array} \right] \\ +\mathbf{H}_4(c\Delta t)^2\mathbf{p}_x^n\left(i,j,k+\frac{1}{2}\right) \end{array} \right\}, \tag{17}$$

and

$$\mathbf{u}_2^{n+1}\left(i,j,k+\frac{1}{2}\right) = \frac{1}{1+\Delta t d_y(j)} \left\{ \begin{array}{l} [2-\Delta t^2 d_y(j)^2]\mathbf{u}_2^n\left(i,j,k+\frac{1}{2}\right) \\ +[\Delta t d_y(j)-1]\mathbf{u}_2^{n-1}\left(i,j,k+\frac{1}{2}\right) \\ +\mathbf{H}_4\alpha_y \left[\begin{array}{l} \mathbf{u}^n\left(i,j+1,k+\frac{1}{2}\right) \\ -2\mathbf{u}^n\left(i,j,k+\frac{1}{2}\right) \\ +\mathbf{u}^n\left(i,j-1,k+\frac{1}{2}\right) \end{array} \right] \\ +\mathbf{H}_4(c\Delta t)^2\mathbf{p}_y^n\left(i,j,k+\frac{1}{2}\right) \end{array} \right\}, \tag{18}$$

where

$$\left\{ \begin{array}{l} \mathbf{p}_x^n\left(i,j,k+\frac{1}{2}\right) = \left\{-\frac{\partial d_x(x)}{\partial x}\exp[-d_x(x)t] * \frac{\partial \mathbf{u}}{\partial x}\right\}^n_{\left(i,j,k+\frac{1}{2}\right)} \\ \mathbf{p}_y^n\left(i,j,k+\frac{1}{2}\right) = \left\{-\frac{\partial d_y(y)}{\partial y}\exp[-d_y(y)t] * \frac{\partial \mathbf{u}}{\partial y}\right\}^n_{\left(i,j,k+\frac{1}{2}\right)} \end{array} \right., \tag{19}$$

and

$$\mathbf{H}_4 = (\mathbf{\Lambda}_1 + \mathbf{\Lambda}_2)^{-1}\mathbf{\Lambda}_2. \tag{20}$$

The time convolution terms in equation 19 can be approximated by the recursion (Wang and Tang, 2003)

$$\left\{ \begin{array}{l} \mathbf{p}_x^n = \exp[-d_x(x)\Delta t]\mathbf{p}_x^{n-1} - \frac{1}{2}\frac{\partial d_x(x)}{\partial x}\Delta t\left[\exp[-d_x(x)\Delta t]\left(\frac{\partial \mathbf{u}}{\partial x}\right)^{(n-1)} + \left(\frac{\partial \mathbf{u}}{\partial x}\right)^{(n)}\right] \\ \mathbf{p}_y^n = \exp[-d_y(y)\Delta t]\mathbf{p}_y^{n-1} - \frac{1}{2}\frac{\partial d_y(y)}{\partial y}\Delta t\left[\exp[-d_y(y)\Delta t]\left(\frac{\partial \mathbf{u}}{\partial y}\right)^{(n-1)} + \left(\frac{\partial \mathbf{u}}{\partial y}\right)^{(n)}\right] \end{array} \right.. \tag{21}$$

The next task is to obtain the discrete formula for calculating the third split component $\mathbf{u}_3$. Considering that a little change is necessary to reach that, we discuss the derivation in detail. The third formula of equation 10 can be approximated discretely by

$$\begin{aligned} &\frac{1}{c}(\mathbf{\Lambda}_1+\mathbf{\Lambda}_2)\frac{\mathbf{u}_3^{n+1}\left(i,j,k+\frac{1}{2}\right) - 2\mathbf{u}_3^n\left(i,j,k+\frac{1}{2}\right) + \mathbf{u}_3^{n-1}\left(i,j,k+\frac{1}{2}\right)}{\Delta t^2} \\ &= \frac{-\mathbf{d}}{\Delta z \Delta t}\left[u^{n+1}\left(i,j,k+\frac{1}{2}\right) - u^{n+1}(i,j,k) - u^{n-1}\left(i,j,k+\frac{1}{2}\right) + u^{n-1}(i,j,k)\right]. \end{aligned} \tag{22}$$

Because the unknown variables $\mathbf{u}_3^{n+1}(i,j,k+\frac{1}{2})$ and $u^{n+1}(i,j,k+\frac{1}{2})$ appear on both sides of equation 22, $\mathbf{u}_3^{n+1}(i,j,k+\frac{1}{2})$ cannot be calculated directly. Change equation 22 equivalently as follows

$$\begin{aligned} &\frac{1}{c}(\mathbf{\Lambda_1}+\mathbf{\Lambda_2})\frac{\mathbf{u}_3^{n+1}\left(i,j,k+\frac{1}{2}\right) - 2\mathbf{u}_3^n\left(i,j,k+\frac{1}{2}\right) + \mathbf{u}_3^{n-1}\left(i,j,k+\frac{1}{2}\right)}{\Delta t^2} \\ &= \frac{-\mathbf{d}}{\Delta z \Delta t}\left[-u^{n+1}(i,j,k) - u^{n-1}\left(i,j,k+\frac{1}{2}\right) + u^{n-1}(i,j,k)\right] - \frac{\mathbf{D}}{\Delta z \Delta t}\mathbf{u}^{n+1}\left(i,j,k+\frac{1}{2}\right) \\ &= \frac{-\mathbf{d}}{\Delta z \Delta t}\left[-u^{n+1}(i,j,k) - u^{n-1}\left(i,j,k+\frac{1}{2}\right) + u^{n-1}(i,j,k)\right] \\ &\quad - \frac{\mathbf{D}}{\Delta z \Delta t}\left[\mathbf{u}_1^{n+1}\left(i,j,k+\frac{1}{2}\right) + \mathbf{u}_2^{n+1}\left(i,j,k+\frac{1}{2}\right) + \mathbf{u}_3^{n+1}\left(i,j,k+\frac{1}{2}\right)\right]. \end{aligned} \tag{23}$$

Rearrangement of equation 23 for $\mathbf{u}_3^{n+1}(i,j,k+\frac{1}{2})$ yields

$$\mathbf{u}_3^{n+1}\left(i,j,k+\frac{1}{2}\right) = \mathbf{H}_2\left[2\mathbf{u}_3^{n}\left(i,j,k+\frac{1}{2}\right) - \mathbf{u}_3^{n-1}\left(i,j,k+\frac{1}{2}\right)\right] + \mathbf{h}_1\left[u^{n+1}(i,j,k) - u^{n-1}(i,j,k) + u^{n-1}\left(i,j,k+\frac{1}{2}\right)\right] - \alpha_z\mathbf{L}\mathbf{D}\left[\mathbf{u}_1^{n+1}\left(i,j,k+\frac{1}{2}\right) + \mathbf{u}_2^{n+1}\left(i,j,k+\frac{1}{2}\right)\right]. \quad (24)$$

Equation 24 is the final expression for updating $\mathbf{u}_3$. Obviously, the calculation of $\mathbf{u}_3$ requires the value of the first two components $\mathbf{u}_1$ and $\mathbf{u}_2$. They should be calculated first, respectively, using equations 17 and 18. Subsequently $\mathbf{u}_3$ can be updated using equation 24. After that, the vector $\mathbf{u}$ is obtained by summing the three split components. The value of integral node in the z-axis is attained in the same way as described by equation 16.

Equations 17, 18, and 24 are the discrete difference scheme for the split PML formulation. As usually seen in the split PML formulation for the full wave equation, by directly summing all the split components, the split scheme used in the PML regions should recover to the original nonsplit scheme used in the interior region. That is the basic requirement of perfectly matching. However, it seems a little different here. It is easy to find by directly setting the damping functions zeros in equations 17 and 18 and then add them to equation 24, the nonsplit scheme 13 cannot be obtained. Does it mean that the derived PML condition does not perfectly match the interior region? In fact, the split scheme can directly return to the nonsplit scheme represented by equation 12 rather than the final form, i.e., equation 13.

With setting $d_x(x) \equiv 0$, $d_y(y) \equiv 0$, and eliminating $\mathbf{p}_x$ and $\mathbf{p}_y$, equations 17 and 18 become

$$(\mathbf{\Lambda}_1 + \mathbf{\Lambda}_2)\mathbf{u}_1^{n+1}\left(i,j,k+\frac{1}{2}\right) = (\mathbf{\Lambda}_1 + \mathbf{\Lambda}_2)\left[2\mathbf{u}_1^{n}\left(i,j,k+\frac{1}{2}\right) - \mathbf{u}_1^{n-1}\left(i,j,k+\frac{1}{2}\right)\right] + \alpha_x\mathbf{\Lambda}_2\left[\mathbf{u}^{n}\left(i+1,j,k+\frac{1}{2}\right) - 2\mathbf{u}^{n}\left(i,j,k+\frac{1}{2}\right) + \mathbf{u}^{n}\left(i-1,j,k+\frac{1}{2}\right)\right], \quad (25)$$

and

$$(\mathbf{\Lambda}_1 + \mathbf{\Lambda}_2)\mathbf{u}_2^{n+1}\left(i,j,k+\frac{1}{2}\right) = (\mathbf{\Lambda}_1 + \mathbf{\Lambda}_2)\left[2\mathbf{u}_2^{n}\left(i,j,k+\frac{1}{2}\right) - \mathbf{u}_2^{n-1}\left(i,j,k+\frac{1}{2}\right)\right] + \alpha_y\mathbf{\Lambda}_2\left[\mathbf{u}^{n}\left(i,j+1,k+\frac{1}{2}\right) - 2\mathbf{u}^{n}\left(i,j,k+\frac{1}{2}\right) + \mathbf{u}^{n}\left(i,j-1,k+\frac{1}{2}\right)\right]. \quad (26)$$

Equation 24 can be rewritten as

$$(\mathbf{\Lambda}_1 + \mathbf{\Lambda}_2 + \alpha_z\mathbf{D})\mathbf{u}_3^{n+1}\left(i,j,k+\frac{1}{2}\right) = (\mathbf{\Lambda}_1 + \mathbf{\Lambda}_2)\left[2\mathbf{u}_3^{n}\left(i,j,k+\frac{1}{2}\right) - \mathbf{u}_3^{n-1}\left(i,j,k+\frac{1}{2}\right)\right] + \alpha_z\mathbf{d}\left[u^{n+1}(i,j,k) - u^{n-1}(i,j,k) + u^{n-1}\left(i,j,k+\frac{1}{2}\right)\right] - \alpha_z\mathbf{D}\left[\mathbf{u}_1^{n+1}\left(i,j,k+\frac{1}{2}\right) + \mathbf{u}_2^{n+1}\left(i,j,k+\frac{1}{2}\right)\right]. \quad (27)$$

By adding the term $\alpha_z\mathbf{D}\mathbf{u}_1^{n+1}(i,j,k+\frac{1}{2})$ to equation 25 and $\alpha_z\mathbf{D}\mathbf{u}_2^{n+1}(i,j,k+\frac{1}{2})$ to equation 26, and then summing the above three equations, we obtain equation 12 again. Therefore, the split scheme used in the PML regions still matches the inner nonsplit scheme.

Different from its counterpart for full wave equation, the split scheme applied here results in a sequence of updating the split components. The component involving the axis that represents the directional property of one-way propagator should be calculated after the other components. Regarding the stability of the explicit difference scheme adopted in this paper, with the help of numerical examples we illustrate the split and nonsplit schemes are conditionally stable.

NUMERICAL EXAMPLES

In this section, we reach two goals through numerical examples: (1) checking the performance of the derived PML condition, including comparison with the wave equation-based CE2 and HABC; (2) observing the stability of the nonsplit scheme used in the interior region and the split scheme used in PML regions.

Goal 1: Comparison of absorption effect and efficiency

Applying CE2 and HABC to 3D AWWE with finite-difference method needs additional attention to treat the corners. It is outside the scope of this paper. As a result, we only use 2D examples to compare their absorption effects and computational efficiency with the developed PML condition. The corresponding 2D PML formulation can be obtained by directly eliminating the y-component. At first, wavefield in a homogeneous medium with a velocity of $c = 2000$ m/s is modeled using AWWE_2 with two reference velocities $(c, 4c)$. CE2, a three-layer HABC, and a twenty-layer PML are, respectively, used as ABCs in the simulation. The damping function in the PML layers takes the form (Collino and Tsogka, 2001)

$$d_x(x) = \frac{3c_{\max}}{2\delta}\log\left(\frac{1}{R}\right)\left(\frac{x}{\delta}\right)^2, \quad (28)$$

where R is the reflection coefficient and δ is the thickness of PML. Quantity $c_{\max}$ is determined as the maximum velocity of the medium. We select $R = 10^{-4}$ and $\delta = 20\Delta x$. A relatively fine grid of $(\Delta x, \Delta z, \Delta t) = (3\text{ m}, 3\text{ m}, 0.5\text{ ms})$ is used. The excitation source takes the form

$$f(x,t) = \exp[-0.05(x-x_o)^2][1 - 2\beta(t-t_0)^2]\exp[-\beta(t-t_0)^2], \quad (29)$$

where $\beta = (\pi f_0)^2$, f_0 is the dominant frequency of the source, and $t_0 = 1/f_0$ is the time corresponding to the peak amplitude. The point (x_o, z_o) represents the location of the excitation source. We set $x_o = 0.5x_{\max}$ and $z_o = 20\Delta z$ where $x_{\max}$ is the lateral size of the computational domain.

Figure 1 shows a series of snapshots gained by a factor of five in amplitude displaying. For a clear contrast, in the left column of Figure 1 CE2 is used on the left edge and PML is used on the right edge, whereas in the right column HABC is used on the left edge and PML on the right edge. Figure 1a is the snapshot at 207.5 ms showing the waves are to impinge the boundaries. Note that the Y-shaped waveforms are evanescent waves which are common in AWWE modeling. Figure 1b is the snapshot at 410 ms, in which some obvious reflections arise at the boundary with CE2, but no obvious ones appear from the boundaries with HABC and PML. Figure 1c is the snapshots at 612.5 ms in which the incident angles to the boundaries are relatively large, so that the low-order CE2 almost loses its absorption function. However, HABC and PML achieve a better absorption, but some weak reflections still can be seen in the HABC and PML scheme. Compared with HABC, PML appears to be more effective to absorb the evanescent waves, but less effective to absorb the propagating waves with a relatively large incident angle (see the white arrows in the right column of Figure 1c for comparison).

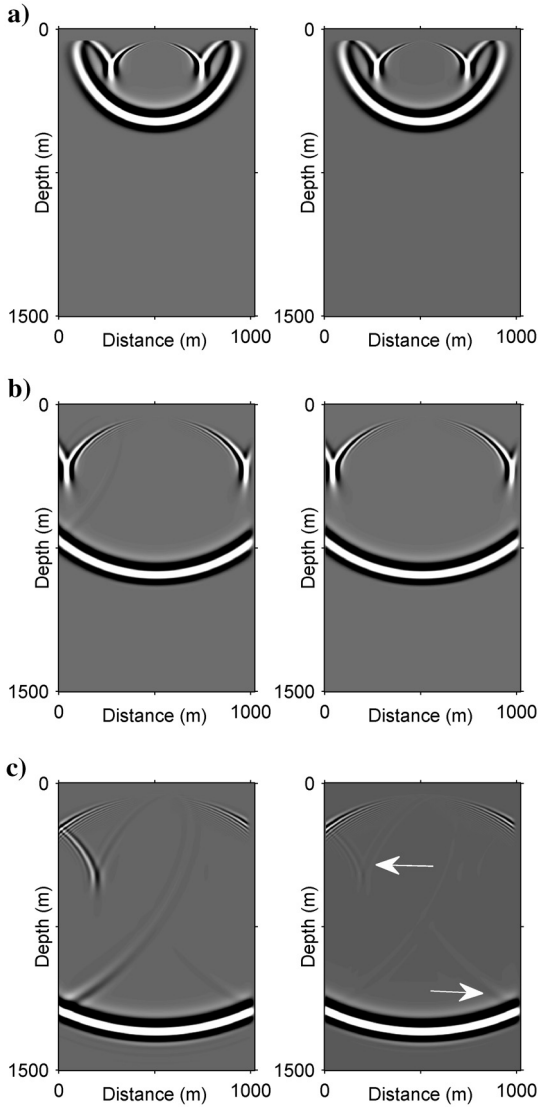

Figure 1. Snapshots propagated by AWWE$_2$ with two reference velocities $(c, 4c)$ in a homogenous medium. CE2, HABC, and PML are used as ABC for comparison. For a clear contrast, in the left column CE2 is used on the left edge and PML is used on the right edge, whereas in the right column HABC is used on the left edge and PML on the right edge. All the snapshots are gained by a factor of five in amplitude dispalying. (a) (b) and (c) are, respectively the snapshots at 207.5, 410, and 612.5 ms.

The difference of absorption effects between the PML scheme and the two wave equation-based ABCs are further illustrated by Figure 2 which is obtained by repeating the forward modeling conducted in Figure 1. This time, the same ABC is used on both edges of the computational domain. Seismograms of two receivers (R1 and R2) are recorded. R1 is located at bottom left of the source with a lateral distance of 418 m and a vertical distance of 412 m. According to the results of Figure 1, the evanescent waves are strong at this depth, so we use R1 to check the absorption effects of the three different ABCs for this wave mode. R2 is right underneath R1 at a deeper depth of 1077 m, where the evanescent waves are weak. We use this receiver to check the performance of the three ABCs for the propagating waves with a relatively large incident angle. The reference solution is obtained by extending the computational domain. Figure 2a is the seismogram of R1, and Figure 2b is the local closer look of Figure 2a. The ripples after about 0.5 s are reflected evanescent waves. It is obvious that PML has achieved a better absorption effect for the evanescent waves than CE2 and HABC. Figure 2c and 2d are, respectively, the seismogram of R2 and its partial enlargement. The ripples that closely follow the direct wave are the reflected propagating waves. It indicates that HABC has achieved a better absorption for the propagating waves with a relatively large incident angle.

A wavefield simulation in 2D Marmousi model (Figure 3) is also conducted to compare the absorption effects and computational efficiency of the derived PML scheme with those of the existing HABC. The total number of grid nodes is 737×750 and 10,000 time steps are executed. A grid size of (6 m, 3 m) with a time increment 0.6 ms is used. The excitation source is located closely to the left boundary. Several snapshots are displayed in Figure 4. Figure 4a is the snapshot at 348 ms and Figure 4b–4f shows the snapshots at 1272 ms. In Figure 4b, the truncation boundary is kept rigid, so obvious edge reflections generate. The bad situation is significantly improved in Figure 4c and 4d where HABC and PML are, respectively used as ABC. The snapshot in Figure 4c is gained by a factor of 10 and redisplayed in Figure 4e. The snapshot in Figure 4d is also gained by a same factor and redisplayed in Figure 4f. It is easy to find that the PML scheme absorbs the evanescent waves much cleaner than HABC (see the white circle in Figure 4e for a comparison).

Actually, the numerical results agree with the conclusion already recognized by Guddati and Lim (2006) that those high-order ABCs using a purely imaginary coordinate stretching are more accurate

for the propagating waves than PML with a complex coordinate stretching, whereas the PML scheme with a complex stretching can simultaneously absorb the propagating and evanescent waves.

Next, the computational efficiency of the developed PML and HABC is also compared through simulating 2D Marmousi model (Figure 3). We use $AWWE_2$ (one auxiliary variable and two reference velocities) to implement the forward modeling, and use HABC and PML as absorbing boundary conditions, respectively. All the calculations are repeated twenty times to get the average of computing time for comparison. With respect to computational scheme without ABC, the simulation using a twenty-layer PML increases the computing time by a factor of 24.4%, and the modeling with a three-layer HABC increases the computing time by a factor of 13.2%. Therefore, the PML scheme seems to be inferior to HABC in computational efficiency.

Goal 2: Observation of stability

A long time (100,000 time steps) simulation is conducted to confirm that the split scheme (equations 25, 26, and 27) is numerically

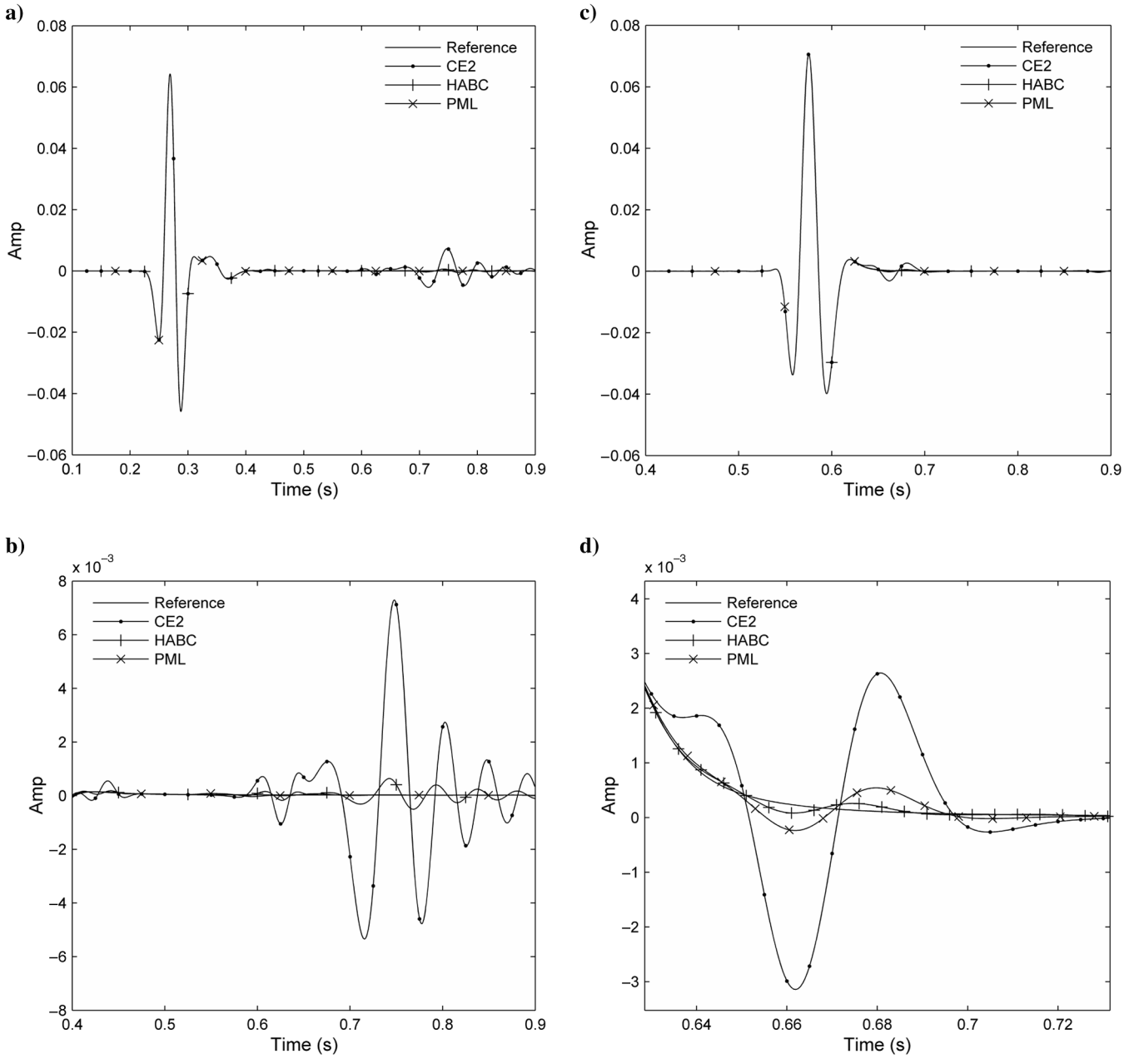

Figure 2. Seismograms of two receivers (R1 and R2). R1 is located at bottom left of the excitation source, and R2 is right underneath R1 at a deeper depth. R1 is used to check absorption effects of the three different ABCs for the evanescent wave mode, and R2 is used to check absorption effects for the propagating wave mode. (a) and (b) are the seismogram of R1 and its partial enlargement, whereas (c) and (d) are the seismogram of R2 and its partial enlargement.

equivalent to the nonsplit scheme (equation 13). As we stress earlier, the numerical consistency is a basic requirement of perfectly matching. The wavefield in a homogenous medium with a velocity of $c = 2000$ m/s is calculated by AWWE$_2$ with a grid size of (4 m, 4 m) and a time step of 0.5 ms. The simulation is first carried out using the nonsplit scheme, and then repeated using the split scheme. In both cases, three receivers are used to record the seismograms for comparison. To exclude the effect of boundary condition, in split and nonsplit cases, the boundaries are kept rigid. Figure 5a displays the seismograms of three different receivers. The seismograms of the nonsplit and split schemes are presented together and their difference is displayed in Figure 5b. Obviously, the numerical discrepancy generated in such a long run between the split and nonsplit schemes is negligible.

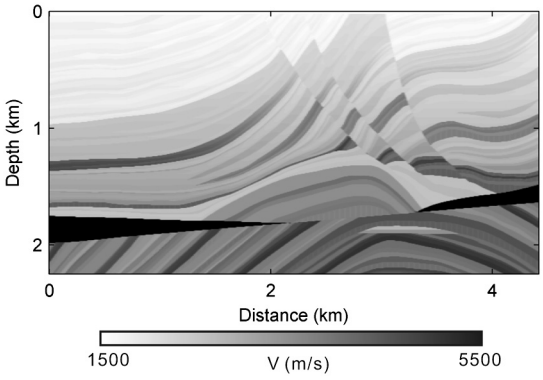

Figure 3. Two-dimensional Marmousi model. The total number of grid nodes is 737×750 with a grid size of $(\Delta x, \Delta z) = (6\text{ m}, 3\text{ m})$.

Regarding stability of the explicit difference scheme adopted in this paper, we give out an empirical restrictive condition, $c\Delta t \le \Delta x$ for 2D case and $\sqrt{2}c\Delta t \le \min(\Delta x, \Delta y)$ for 3D case, which is different from the condition $c\Delta t \le \min(\Delta x, \Delta z)$ for 2D case presented by Guddati and Heidari (2005).

Extensive numerical examples have been conducted to prove that it is safe for the split and nonsplit schemes when the empirical restrictive condition is satisfied. Partial results are listed in Table 1 which is obtained by calculating the wavefield using AWWE$_2$ in 2D Marmousi model (Figure 3). The maximum velocity in the original model is modified to be 5000 m/s. The time increment is 0.2 ms, such that $c\Delta t \equiv 1.0$. Twenty thousand time steps with various grid sizes are executed to observe the stability. It seems to be safe to get three points from Table 1. First, the stability is independent of the grid vertical size. Second, the split and nonsplit scheme probably share the same stability condition. That means when the interior nonsplit scheme is stable, the split scheme in the PML regions is also stable. Meanwhile, when the nonsplit scheme is unstable, the split scheme is also unstable. In addition, the stability is slightly affected by the reference velocities. Fortunately, when the suggested empirical restrictive condition $c\Delta t \le \Delta x$ is met, the nonsplit and split schemes can obtain a stable result, no matter how the reference velocities are set.

Note that the examples listed here are only a small part of those extensive numerical examples we have implemented. A rigorous analysis on the stability is under consideration but not included in this paper.

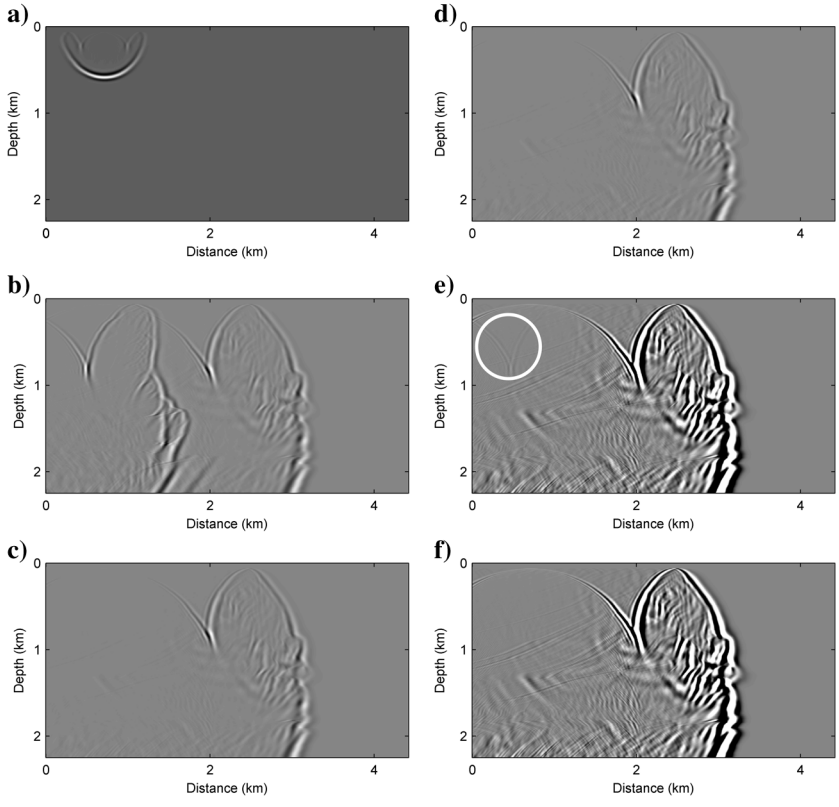

Figure 4. Snapshots propagated by AWWE$_2$ in 2D Marmousi model with different ABCs. (a) is the snapshot at 348 ms and (b-f) are the snapshots at 1272 ms. In (b), the boundary is rigid, in (c) HABC is used, and in (d) PML is used. (e) and (f) are, respectively obtained by gaining (c) and (d) in amplitude displaying by a factor of 10. The white circle in (e) points out the uncleanly absorbed evanescent waves by HABC.

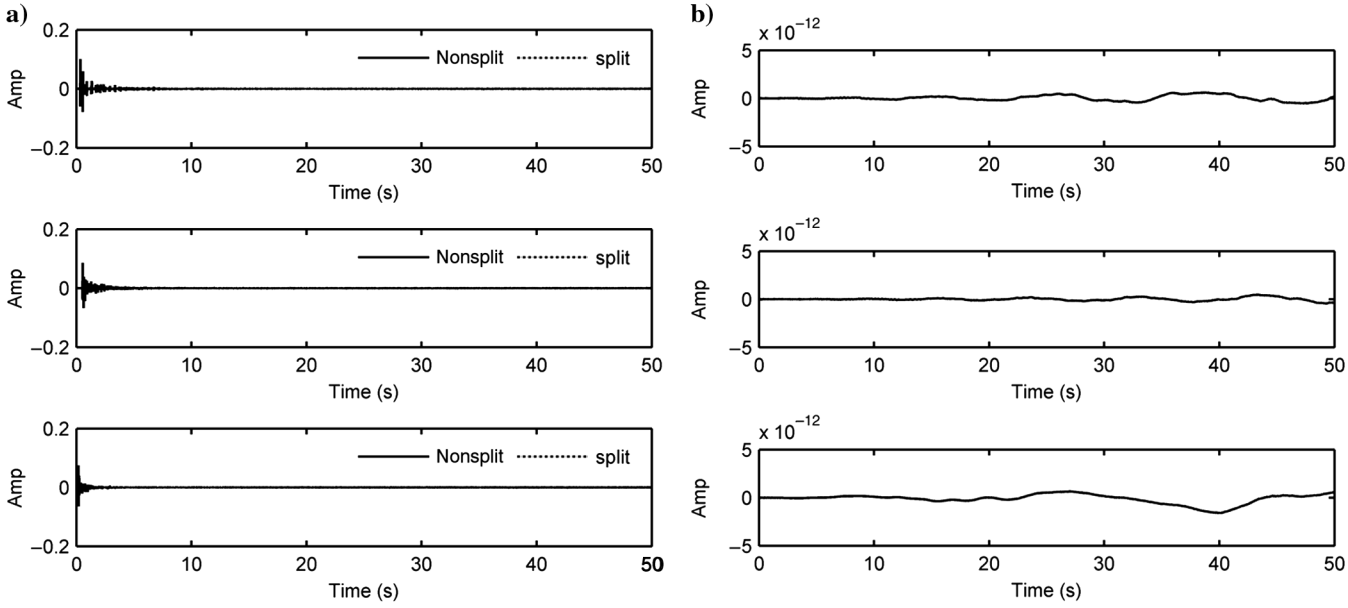

Figure 5. A long simulation (100,000 time steps) is conducted in a homogenous medium with a velocity of 2000 m/s to present the numerical discrepancy between the split and nonsplit schemes. The boundaries are rigid to exclude the effects of boundary conditions. (a) displays the seismograms of three receivers, and (b) displays the difference between the split and nonsplit schemes.

Table 1. Observing the stability of the nonsplit and split schemes with various grid sizes ($c\Delta t \equiv 1$).

Grid size $(\Delta x, \Delta z)$	Nonsplit			Split		
	(c, c)	$(c, 2c)$	$(c, 4c)$	(c, c)	$(c, 2c)$	$(c, 4c)$
(5 m, 1 m)	Stable	Stable	Stable	Stable	Stable	Stable
(5 m, 0.5 m)	Stable	Stable	Stable	Stable	Stable	Stable
(5 m, 0.1 m)	Stable	Stable	Stable	Stable	Stable	Stable
(0.99 m, 3 m)	Stable	Stable	Stable	Stable	Stable	Stable
(0.98 m, 3 m)	Stable	Stable	Unstable	Stable	Stable	Unstable
(0.96 m, 3 m)	Stable	Unstable	Unstable	Stable	Unstable	Unstable
(0.92 m, 3 m)	Unstable	Unstable	Unstable	Unstable	Unstable	Unstable

Finally, a 3D example is given out to check the performance of the derived PML condition. The 3D inhomogeneous model (Figure 6) is generated by truncating the 2D Marmousi model (Figure 3) and then stretching along the x-axis. A grid size of $(\Delta x, \Delta y, \Delta z) = (8\text{ m}, 8\text{ m}, 4\text{ m})$ and a time step $\Delta t = 1$ ms are used. The excitation source is located at a depth of 0 m and in the center of xoy-plane. Five thousand time steps are executed. PML layers are used as ABC perpendicularly to x- and y-axis. Considering our main purpose is to check the absorption effect in the corners, several 2D snapshots recorded at a xoy-section at a depth of 500 m are presented and other sections are not shown here. Figure 7a–7d shows, respectively, snapshots at 300 ms, 550 ms, 1130 ms, and 5 s. The heterogeneity of the model complicates the wavefield, including some lateral reflections. However, the energy nearby the corners is always weak, indicating the PML scheme achieves a desirable performance in the corners.

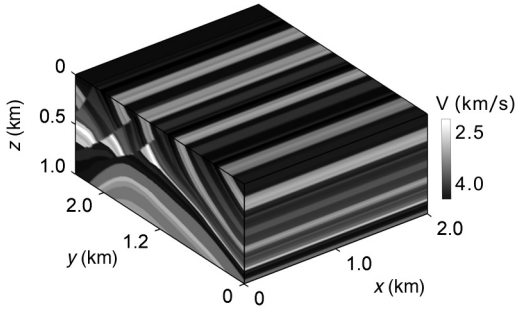

Figure 6. Three-dimensional inhomogeneous model. The size is (2000 m, 2400 m, 1000 m).

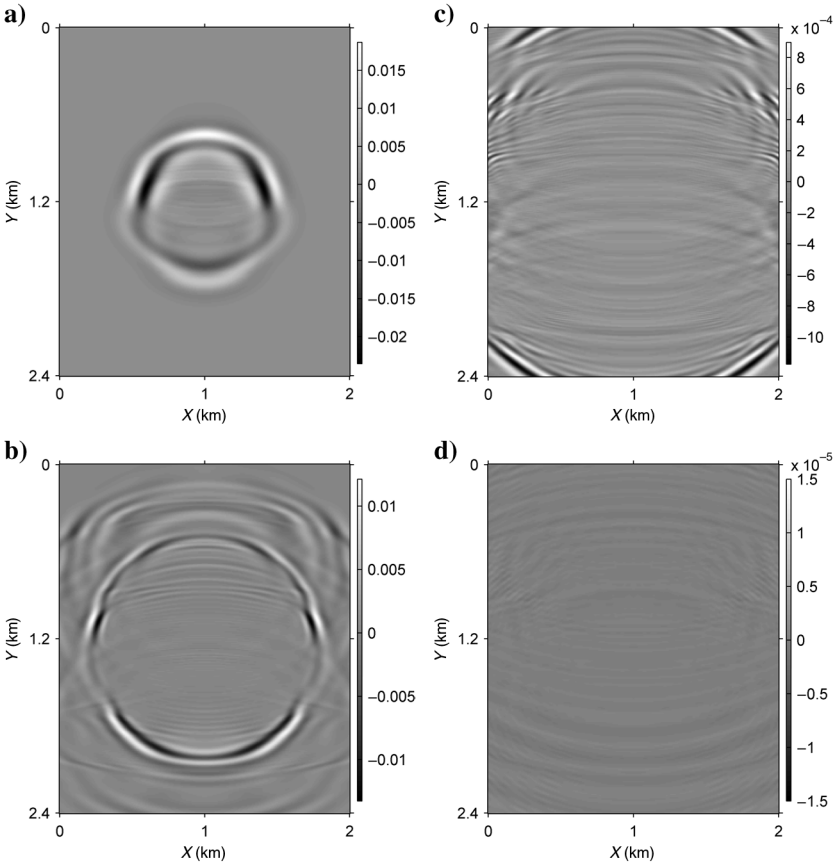

Figure 7. Several 2D snapshots of the *xoy*-section at a depth of 500 m. The excitation source is located at a depth of 0 m and at the center of *xoy*-plane. Note that the *xoy*-section simultaneously includes PML layers parallel to the *x*- and *y*-axis, so it is convenient to check absorption effects in the corners. (a–d) are, respectively, snapshots at 300 ms, 550 ms, 1130 ms, and 5 s.

CONCLUSIONS

We derive a split PML formulation for 3D scalar AWWEs, offering a good approach to suppress the edge reflections in AWWE forward modeling and migration. The essence of PML, i.e., a complex coordinate stretching, is rehashed in our derivation procedure. An existing finite-difference scheme is adopted to fit the split PML formulation. Some typical numerical examples are presented to show that the developed PML condition can achieve a better absorption effect for the evanescent waves and an almost identical absorption effect for the propagating waves, compared with an existing high-order ABC. Although a little more computing time is required in the PML scheme than the existing ABC, extending the PML condition to a 3D case with finite-difference method is more direct. Meanwhile, considering the PML scheme can effectively absorb the evanescent waves that are common in AWWE forward modeling, the developed PML condition is another good choice. Numerical examples indicate that the usage of the split PML formulation in AWWE forward modeling does not generate any additional instability when an empirical restrictive condition is met. We find the stability condition of the explicit difference scheme adopted in this paper seems to be independent of vertical grid size and slightly related to the reference velocities. These interesting issues will be discussed in detail in our future work.

ACKNOWLEDGMENTS

This work was supported in part by the 973 Program of China (2013CB228603), National Major Science and Technology Program (2011ZX05010-001, 2011ZX05024-001), and the Research of Novel Method and Technology of Geophysical Prospecting, CNPC (2011A-3602). We are also grateful to Dr. Sanyi Yuan for constructive advice and helpful discussion.

REFERENCES

Asvadurov, S., V. Druskin, M. N. Guddati, and L. Knizhnerman, 2003, On optimal finite-difference approximation of PML: SIAM Journal on Numerical Analysis, **41**, 287–305, doi: 10.1137/S0036142901391451.

Bakker, P. M., 2009, A stable one-way wave propagator for VTI media: Geophysics, **74**, no. 5, WB3–WB17, doi: 10.1190/1.3196818.

Bamberger, A., B. Engquist, L. Halpern, and P. Joly, 1988, High-order paraxial wave-equation approximation in heterogeneous media: SIAM Journal on Applied Mathematics, **48**, 129–154, doi: 10.1137/0148006.

Baysal, E., D. D. Kosloff, and J. W. C. Sherwood, 1983, Reverse time migration: Geophysics, **48**, 1514–1524, doi: 10.1190/1.1441434.

Bérenger, J. P., 1994, A perfectly matched layer for the absorption of electromagnetic waves: Journal of Computational Physics, **114**, 185–200, doi: 10.1006/jcph.1994.1159.

Berkhout, A. J., 1979, Steep dip finite-difference migration: Geophysical Prospecting, **27**, 196–213, doi: 10.1111/gpr.1979.27.issue-1.

Biondi, B., 2002, Stable wide-angle Fourier finite-difference downward extrapolation of 3-D wavefields: Geophysics, **67**, 872–882, doi: 10.1190/1.1484530.

Chew, W. C., and W. H. Weedon, 1994, A 3D perfectly matched medium from modified Maxwell's equations with stretched coordinates: Microwave and Optical Technology Letters, **7**, 599–604, doi: 10.1002/(ISSN)1098-2760.

Claerbout, J. F., 1985, Imaging the Earth's interior: Blackwell Scientific Publications Inc.

Clayton, R. W., and B. Engquist, 1977, Absorbing boundary conditions for acoustic and elastic wave equations: Bulletin of the Seismological Society of America, **6**, 1529–1540.

Clayton, R. W., and B. Engquist, 1980, Absorbing boundary conditions for wave-equation migration: Geophysics, **45**, 895–904, doi: 10.1190/1.1441094.

Collino, F., 1997, Perfectly matched absorbing layers for the paraxial equations: Journal of Computational Physics, **131**, 164–180, doi: 10.1006/jcph.1996.5594.

Collino, F., and C. Tsogka, 2001, Application of the PML absorbing layer model to the linear elastodynamic problem in anisotropic heterogeneous media: Geophysics, **66**, 294–307, doi: 10.1190/1.1444908.

Collins, M. D., and E. K. Westwood, 1991, A higher-order energy-conserving parabolic equation for range-dependent ocean depth, sound speed, and density: Journal of the Acoustical Society of America, **89**, 1068–1175, doi: 10.1121/1.400526.

Engquist, B., and A. Majda, 1977, Absorbing boundary conditions for numerical simulation of waves: Applied Mathematical Sciences, **74**, 1765–1766.

Gazdag, J., 1978, Wave equation migration with the phase-shift method: Geophysics, **43**, 1342–1351, doi: 10.1190/1.1440899.

Gazdag, J., and P. Sguazzero, 1984, Migration of seismic data by phase-shift plus interpolation: Geophysics, **49**, 124–131, doi: 10.1190/1.1441643.

Givoli, D., 2004, High-order local non-reflecting boundary conditions: A review: Wave Motion, **39**, 319–326, doi: 10.1016/j.wavemoti.2003.12.004.

Givoli, D., and B. Neta, 2003, High-order non-reflecting boundary scheme for time-dependent waves: Journal of Computational Physics, **186**, 24–46, doi: 10.1016/S0021-9991(03)00005-6.

Grote, M. J., and J. B. Keller, 1996, Nonreflecting boundary conditions for time dependent scattering: Journal of Computational Physics, **127**, 52–65, doi: 10.1006/jcph.1996.0157.

Guddati, M. N., 2006, Arbitrarily wide-angle wave equations for complex media: Computer Methods in Applied Mechanics and Engineering, **195**, 65–93, doi: 10.1016/j.cma.2005.01.006.
Guddati, M. N., and A. H. Heidari, 2005, Migration with arbitrarily wide-angle wave equations: Geophysics, **70**, no. 3, S61–S70, doi: 10.1190/1.1925747.
Guddati, M. N., and K.-W. Lim, 2006, Continued fraction absorbing boundary conditions for convex polygonal domains: International Journal for Numerical Methods in Engineering, **66**, 949–977, doi: 10.1002/(ISSN)1097-0207.
Guddati, M. N., and J. L. Tassoulas, 2000, Continued-fraction absorbing boundary conditions for the wave equation: Journal of Computational Acoustics, **8**, 139–156, doi: 10.1016/S0218-396X(00)00009-1.
He, B., H. Zhang, and J. Zhang, 2008, Prestack reverse-time depth migration of arbitrarily wide-angle wave equations: Acta Seismologica Sinica, **20**, 492–501, doi: 10.1007/s11589-008-0492-x.
Heidari, A. H., and M. N. Guddati, 2006, Highly accurate absorbing boundary conditions for wide-angle wave equations: Geophysics, **71**, no. 3, S85–S97, doi: 10.1190/1.2192914.
Huang, L., and R. Wu, 1996, Prestack depth migration with acoustic screen propagator: 66th Annual International Meeting, SEG, Expanded Abstracts, 415–418.
Jia, X., and R. Wu, 2009, Superwide-angle one-way wave propagator and its application in imaging steep salt flanks: Geophysics, **74**, no. 4, S75–S83, doi: 10.1190/1.3124686.
Jin, S., R. Wu, and C. Peng, 1999, Seismic depth migration with pseudoscreen propagator: Computational Geosciences, **3**, 321–335, doi: 10.1023/A:1011587227696.
Komatitsch, D., and J. Tromp, 2003, A perfectly matched layer absorbing boundary condition for the second-order seismic wave equation: Geophysical Journal International, **154**, 146–153, doi: 10.1046/j.1365-246X.2003.01950.x.
Lee, M. W., and S. Y. Suh, 1985, Optimization of one-way wave equations: Geophysics, **50**, 1634–1637, doi: 10.1190/1.1441853.
Levy, M. F., 2001, Perfectly matched layer truncation for parabolic wave equation models: Proceedings of the Royal Society of London, Series A: Mathematical, Physical and Engineering Sciences, **457**, 2609–2624, doi: 10.1098/rspa.2001.0848.
Lu, Y., and J. Zhu, 2007, Perfectly matched layer for acoustic waveguide modeling-benchmark calculations and perturbation analysis: CMES. Computer Modeling in Engineering & Sciences, **22**, 235–248.
McMechan, G. A., 1983, Migration by extrapolation of time-dependent boundary values: Geophysical Prospecting, **31**, 413–420, doi: 10.1111/gpr.1983.31.issue-3.
Mulder, W. A., and R.-E. Plessix, 2004, A comparison between one-way and two-way wave equation migration: Geophysics, **69**, 1491–1504, doi: 10.1190/1.1836822.
Mur, G., 1981, Absorbing boundary conditions for the finite-difference approximation of the time-domain electromagnetic field equations: IEEE Transactions on Electromagnetic Compatibility, **EMC-23**, 377–382, doi: 10.1109/TEMC.1981.303970.
Ristow, D., and T. Rühl, 1994, Fourier finite-difference migration: Geophysics, **59**, 1882–1893, doi: 10.1190/1.1443575.
Rowley, C. W., and T. Colonius, 2000, Discretely nonreflecting boundary conditions for linear hyperbolic systems: Journal of Computational Physics, **157**, 500–538, doi: 10.1006/jcph.1999.6383.
Shlager, K. L., and J. B. Schneider, 1995, Selective survey of the finite-difference time-domain literature: IEEE Antennas and Propagation Magazine, **37**, 39–57, doi: 10.1109/74.414731.
Stoffa, P. L., J. T. Fokkema, R. M. de Luna Freire, and W. P. Kessinger, 1990, Split-step Fourier migration: Geophysics, **55**, 410–421, doi: 10.1190/1.1442850.
Sun, Q., and Q. Du, 2011, Study on depth migration with arbitrarily wide-angle wave equation: 3rd IEEE International Conference on Communication Software and Networks, 230–233.
Wang, T., and X. Tang, 2003, Finite-difference modeling of elastic wave propagation: A nonsplitting perfectly matched layer approach: Geophysics, **68**, 1749–1755, doi: 10.1190/1.1620648.
Whitmore, N. D., 1983, Iterative depth migration by backward time propagation: 53rd Annual International Meeting, SEG, Expanded Abstracts, 382–385.
Yuan, S., S. Wang, Y. He, and N. Tian, 2011, Second-order wave equation modeling in time domain with surface topography using embedded boundary method and PML: 73rd Annual International Conference and Exhibition, EAGE, Extended Abstracts, 356–360.
Zhang, G., 1985, High-order approximation of one-way wave equations: Journal of Computational Mathematics, **3**, 90–97.
Zhang, Y., S. Xu, and G. Zhang, 2006, Imaging complex salt bodies with turning-wave one-way wave equation: 76th Annual International Meeting, SEG, Expanded Abstracts, 2323–2327.
Zhou, H. B., and G. A. McMechan, 2000, Rigorous absorbing boundary conditions for 3-D one-way wave extrapolation: Geophysics, **65**, 638–645, doi: 10.1190/1.1444760.